



Full Length Article

Predicting hydrogen engine performance with water addition using a two-zone thermodynamic model

D.N. Rrustemi , L.C. Ganippa , T. Megaritis , C.J. Axon ^{*} 

Department of Mechanical and Aerospace Engineering, Brunel University of London, Uxbridge, London UB8 3PH, UK

ARTICLE INFO

Keywords:

Boosting

ICE

Laminar flame speed

Two-zone model

Water dilution

Water injection

ABSTRACT

Hydrogen is an alternative fuel for internal combustion engines, with potential to reduce emissions and improve engine efficiency through boosted lean burn operation. The injection of water into hydrogen-fuelled internal combustion engines could offer the benefit of reducing combustion abnormalities and controlling emissions through in-cylinder thermo-physical property changes. A two-zone combustion model was developed and validated to predict the performance of a boosted lean-burn hydrogen spark ignition engine with water addition. This new thermodynamic model incorporates a water-diluted hydrogen laminar flame speed correlation, an extended Zeldovich mechanism for nitric oxide emissions prediction, and the Livengood-Wu integral model for evaluating knocking characteristics based on advanced chemical kinetics. The study offers a comprehensive analysis of a hydrogen-fuelled internal combustion engine operated at various manifold air pressures, equivalence ratios, and quantity of water addition. The study indicated that addition of water significantly reduces combustion abnormalities and emissions. A 1 % water addition, at an equivalence ratio of 0.9 and manifold absolute pressure of 120 kPa, reduces the knock integral by 2 % and nitric oxide emissions by 5 %. Finally, the study underlines the importance of optimizing the water injection amount to balance the trade-offs between engine performance, fuel consumption, emission reduction, and knocking regions. The model is a tool to develop advanced combustion strategies in hydrogen-fuelled internal combustion engines.

1. Introduction

Environmental constraints and limited fossil reserves have led to the exploration of hydrogen as an alternative fuel for internal combustion engines with the potential to reduce greenhouse gas emissions [1]. Hydrogen has several advantages; its laminar flame speed is four times greater than that of gasoline, leading to faster reactive mixture combustion. The diffusion coefficient of hydrogen is almost four times higher than that of gasoline, potentially leading to improved fuel and air mixing and thus achieving better mixture homogeneity. Furthermore, the hydrogen lean limit is significantly lower compared to that of gasoline. This implies that hydrogen has the potential to operate more effectively when under lean mixtures, thereby offering an effective way to enhance engine efficiency [2]. Although hydrogen has a higher Research Octane Number than gasoline, hydrogen engines are still vulnerable to knocking [3]. Several automotive manufacturers are developing boosted and downsized hydrogen spark ignition (SI) engines to compete with current gasoline engines, as the hydrogen/air mixtures

have lower volumetric energy [4]. It has been demonstrated that by increasing the intake manifold air pressure in a hydrogen-fuelled spark ignition (SI), the power output becomes comparable to that of gasoline engine while consuming significantly less fuel [4]. However, when the equivalence ratio approaches unity, the hydrogen-powered port injection engine faces challenges, as its benefits become limited due combustion abnormalities [5]. Increasing the intake air pressure raises the overall engine in-cylinder pressure, consequently raising the in-cylinder temperature, which significantly increases NO_x emissions. While knock and NO_x emissions can be minimized by optimizing spark timing and compression ratio, these optimization of factors can affect the thermal efficiency of the engine [6]. It has been shown that by retarding the spark timing, the probability of occurrence of pre-ignition increases due to a rise in residual mass temperature [7]. Thus, strategies to reduce the in-cylinder temperature are essential for successful abatement of NO_x production. Strategies to achieve low-temperature combustion (LTC) through the introduction of cooled exhaust gas recirculation (EGR), lean burn operation, as well as water injection have been evaluated for NO_x reduction and knock mitigation [8]. Additionally, the hydrogen-fuelled

* Corresponding author.

E-mail addresses: Dardan.Rrustemi@brunel.ac.uk (D.N. Rrustemi), Lionel.Ganippa@brunel.ac.uk (L.C. Ganippa), Thanos.Megaritis@brunel.ac.uk (T. Megaritis), Colin.Axon@brunel.ac.uk (C.J. Axon).

<https://doi.org/10.1016/j.fuel.2024.134137>

Received 9 August 2024; Received in revised form 8 October 2024; Accepted 17 December 2024

Available online 4 January 2025

0016-2361/© 2024 The Author(s). Published by Elsevier Ltd. This is an open access article under the CC BY license (<http://creativecommons.org/licenses/by/4.0/>).

Nomenclature	
<i>Symbols</i>	
N	engine speed (rpm)
P	in-cylinder pressure (MPa)
Q	heat transfer (J/degree)
T	in-cylinder temperature (K)
U	internal energy (J)
V	volume (m ³)
W	work (J)
θ	crank angle (degree)
ϕ	equivalence ratio
γ	specific heat ratio
τ	autoignition delay
λ	excess air ratio
<i>Acronyms</i>	
AFR	air/fuel ratio
AHRR	apparent heat release rate (J/degree)
aTDC	after top dead centre
bTDC	before top dead centre
CA	crank angle
CA50	location of 50 % mass fraction burned
CO ₂	carbon dioxide
ISFC	indicated specific fuel consumption (kg/kWh)
KI	knock integral
ISFC	indicated specific fuel consumption (kg/kWh)
LFS	laminar flame speed (m/s)
MAP	manifold air pressure (kPa)
NO	nitric oxide
NOx	oxides of nitrogen
SI	spark ignition
ST	spark timing
TDC	top dead centre
<i>Subscripts</i>	
0	initial condition
b	burnt
d	displaced volume
f	fuel
$loss$	heat losses
soc	start of combustion
u	unburned

engine exhaust contains high levels of water vapor. Under EGR operation the water content in the cylinder increases, therefore, it is important to study the effect of water addition into a hydrogen engine.

The injection of water either via intake or through direct injection provides significant cooling of the in-cylinder mixture due to the higher latent heat of vaporization of water, mitigating the combustion abnormalities under higher engine loads [3,9,10]. Investigating the effects of water injection at various spark timings shows that NOx emissions could be significantly reduced with low thermal efficiency losses [11]. Injecting water through the port in a hydrogen direct injection engine achieved a NOx reduction of up to 87 % but with only 2 % fuel consumption penalty [12]. Whereas, for direct injection of water to a port injected hydrogen SI engine, NOx emissions reduced up to 95 % with an 8 % penalty of fuel consumption [13]. The amount and timing of direct water injection is also relevant as the performance of the hydrogen engine decreases with retardation of water injection timing i.e. earlier injection timing of water was proposed for better performance. Moreover, it was shown that the performance of the hydrogen-fuelled SI engine increased with the addition of water (0 to 4.05 mg/cycle) for an excess air ratio of 1.15 [14]. Due to wider flammability limit, hydrogen is capable of allowing high rates of dilution with air, exhaust gas, or water vapour before combustion stability deteriorates [15]. The quantity of water direct injection is independent of the fuel and air flow and can be applied throughout the entire operating range of a hydrogen engine [16].

The exhaust gas composition of hydrogen-fuelled internal combustion engines (ICE) contains significant levels of water vapor, hence it is important to understand the isolated effect of water addition on hydrogen combustion. Besides the thermal and chemical effects of water on the reactive hydrogen mixture, it modulates the laminar flame speed (LFS), which is an important parameter for numerical combustion models to understand ICE processes. Global combustion models are effective in terms of time and cost, and when used appropriately provide useful information regarding combustion and emission performance with a degree of accuracy comparable to more complex multi-dimensional combustion models [17]. An enhanced single-zone thermodynamic model with a LFS sub-model investigated combustion of a boosted lean-burn hydrogen SI engine at various spark timings [6]. Furthermore, the LFS correlations for hydrogen with water addition were recently developed [18]. The addition of water to hydrogen-air

flames under atmospheric conditions has three main effects: 1) dilution, which reduces the net reaction rate, 2) thermal-diffusion, which alters the thermodynamic and transport properties of the reactants, and 3) chemical, which occurs due to the participation of the diluent in elementary kinetic reactions [19]. The LFS values calculated using the empirical correlation can be incorporated into a two-zone combustion model where the chamber is divided into burned and unburned zones [20]. Another influential parameter in numerical combustion studies is heat transfer; the hydrogen engine experiences a significant increase in heat flux compared to carbon-based fuels, so an appropriate heat transfer model must be selected for accurate prediction [21]. If the coefficient of Woschni correlation [22] is properly tuned, hydrogen heat transfer can be accurately predicted [23]. The variations in the thermodynamics of the in-cylinder mixture with water addition can be captured using existing empirical correlations to calculate the specific state properties. [24]. The two-zone combustion model has been used to investigate the water addition effect by capturing the cooling and dilution effects of the added water [25]. In this study, a two-zone water-diluted hydrogen combustion model was developed and extended for various engine operating conditions. Additionally, sub-models for engine knock and NO emissions were implemented to provide a comprehensive study of the performance, combustion abnormalities, and NO emissions of a boosted lean burn hydrogen SI engine under injection water environment.

2. Methodology

A two-zone combustion model was developed and validated to predict the performance of a hydrogen fuelled SI engine with and without water addition under various equivalence ratios and manifold air pressures. The main assumption of this model is the division of the combustion chamber into two zones: the burned zone consisting of combustion products, and the unburned zone consisting of reactants. Both zones are treated as ideal gases, and it is assumed that there is no heat transfer between the zones. The pressure was assumed to be uniform throughout the chamber but the temperatures were differentiated between the burned and unburned zones. Using the conservation of mass and energy, the temperature, pressure, and heat release equations were derived (Appendix A1). The sub-models for knocking and NO emissions of a boosted lean burn hydrogen engine were developed as discussed in

[6].

2.1. Mass fraction

The main input to the two-zone combustion model is the mass fraction burned, and calculated by introducing an entrainment zone that interfaces the burned and unburned zones [26], as shown in Fig. 1. As the kernel initiates from the spark source, it interacts with the turbulent motion of the charge within the cylinder. The laminar flame surface experiences intensive wrinkling due to the in-cylinder turbulence. After a period of transition, the flame becomes entirely turbulent. When the flame expands, the entrainment of the unburned gases also increases, causing the flame to advance faster than the rate at which combustion takes place [27]. The combustion occurs at the laminar burning rate of the fuel, which is determined by the equivalence ratio, pressure, temperature, and water dilution level [18]. The entrainment of the unburned gases caused by the turbulence interactions occurs at a specific burning time, τ . The entrainment mass fraction of the reactive mixture and the actual mass fraction burned were calculated from Eqs. (1) and (2), respectively,

$$\frac{dm_e}{dt} = \rho_u A_f (S_L + u') \quad (1)$$

$$\frac{dm_b}{dt} = \frac{m_e - m_b}{\tau_c} \quad (2)$$

where m_e is the entrained mass, m_b is the burned mass, ρ_u is the hydrogen/air unburned mixture density, A_f is the flame front area, S_L is the hydrogen laminar flame speed, and u' is the turbulence intensity. The flame front area A_f is calculated based on the approach proposed in [28] and later refined in [29]. The characteristic burning time, τ_c , was calculated as the ratio of the Taylor micro-scale length to the laminar flame speed $\tau_c = C_T L_T / S_L$. The hydrogen laminar flame speed with water addition was calculated using the empirical correlation proposed in [18]. The water-diluted hydrogen combustion laminar flame speed correlation developed by the authors of this work in [18] is valid for pressure ranges from 10 to 70 bar, temperatures from 400 to 800 K, equivalence ratios from 0.35 to 1, and for water addition by mole fraction from 0 to 20 %.

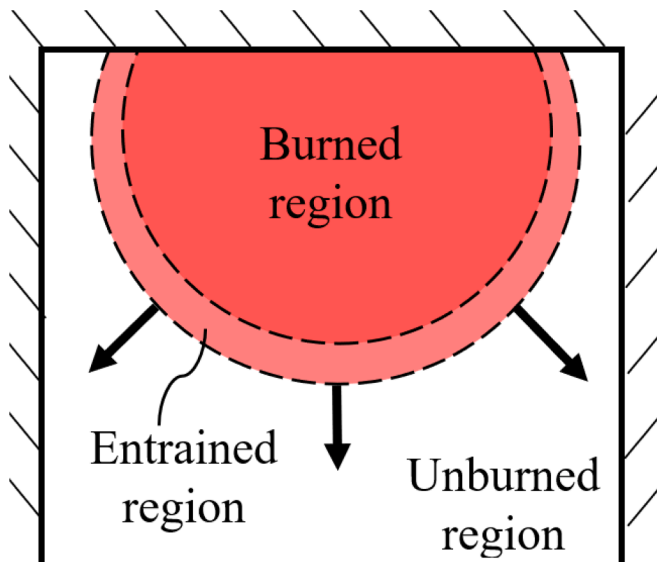


Fig. 1. Conceptual diagram of the combustion model. The entrained region represents the flame front.

2.2. In-cylinder turbulence

Zero-dimensional turbulence modelling is challenging since it aims to replicate complex 3D phenomena. Without spatial information, the most commonly used approach for turbulence modelling is a combined k - ϵ equation. The calculation of the in-cylinder turbulent kinetic energy and its dissipation was calculated by using the established zero-dimensional model [29], as follows:

$$\frac{dk}{dt} = -\frac{2}{3} \frac{k}{\rho} \frac{d\rho}{dt} - \epsilon \quad (3)$$

$$\epsilon = \frac{k^{\frac{3}{2}}}{l_t} \quad (4)$$

The integral turbulent length l_t is calculated based on the approach proposed by [30], where

$$l_t = l_{t,IVC} \sqrt{\frac{k_{EC}}{k}} \quad (5)$$

The integral length scale at IVC, $l_{t,IVC}$, and k_{EC} were taken from dynamic discharge analysis performed using the Converge software [31]. To ensure the functionality of the zero-dimensional turbulence model used in this work, initial turbulent kinetic energy data was generated using three-dimensional CFD data. In Fig. 2, the zero-dimensional and three-dimensional kinetic turbulence energy are compared for manifold air pressures for a premixed hydrogen/air mixture. It can be seen that the zero-dimensional k - ϵ turbulence model was capable of predicting in-cylinder kinetic turbulence energy comparable to an advanced 3D CFD simulation.

2.3. Heat release rate

The heat release based on the first law of thermodynamics is

$$dQ_{ch} = dU + dW + dQ_{loss} \quad (6)$$

The energy change during combustion is equal to the change in internal energy and the work done by the system. The heat release rate during combustion accounting for heat loss is [32]:

$$\frac{dQ}{d\theta} = \frac{\gamma}{\gamma - 1} p \frac{dV}{d\theta} + \frac{1}{\gamma - 1} V \frac{dp}{d\theta} - dQ_{loss} \quad (7)$$

where γ is the specific heat ratio of the mixture, p is the in-cylinder pressure, and V is the instantaneous volume and dQ_{loss} is the convective heat loss. The hydrogen combustion heat loss was modelled using the Woschni correlation [22]. The heat transfer coefficient used in the Woschni equation was multiplied by a factor of 2.2 to match with the actual losses of a hydrogen-fuelled engine [23]. The thermodynamic properties of water-diluted hydrogen at various operating conditions were calculated using the NASA polynomial [24]. The specific heat, and standard state enthalpy were calculated using Eqs. (8)–(9):

$$\frac{c_p(T)}{R} = a_1 + a_2 T + a_3 T^2 + a_4 T^3 + a_5 T^4 \quad (8)$$

$$\frac{h(T)}{R} = a_1 + \frac{a_2 T}{2} + \frac{a_3 T^2}{3} + \frac{a_4 T^3}{4} + \frac{a_5 T^4}{5} + \frac{a_6}{T} \quad (9)$$

The values for the coefficient a_i for H_2 , O_2 , N_2 and H_2O are taken from [24].

2.4. Knock model

Hydrogen SI engines are prone to abnormal combustion phenomena which could be due to auto-ignition of the unburned end-gas mixture or through pre-ignition [14]. Pre-ignition could be caused by the formation of hot spots or by unburned hydrogen left from the previous cycle [7]. Li

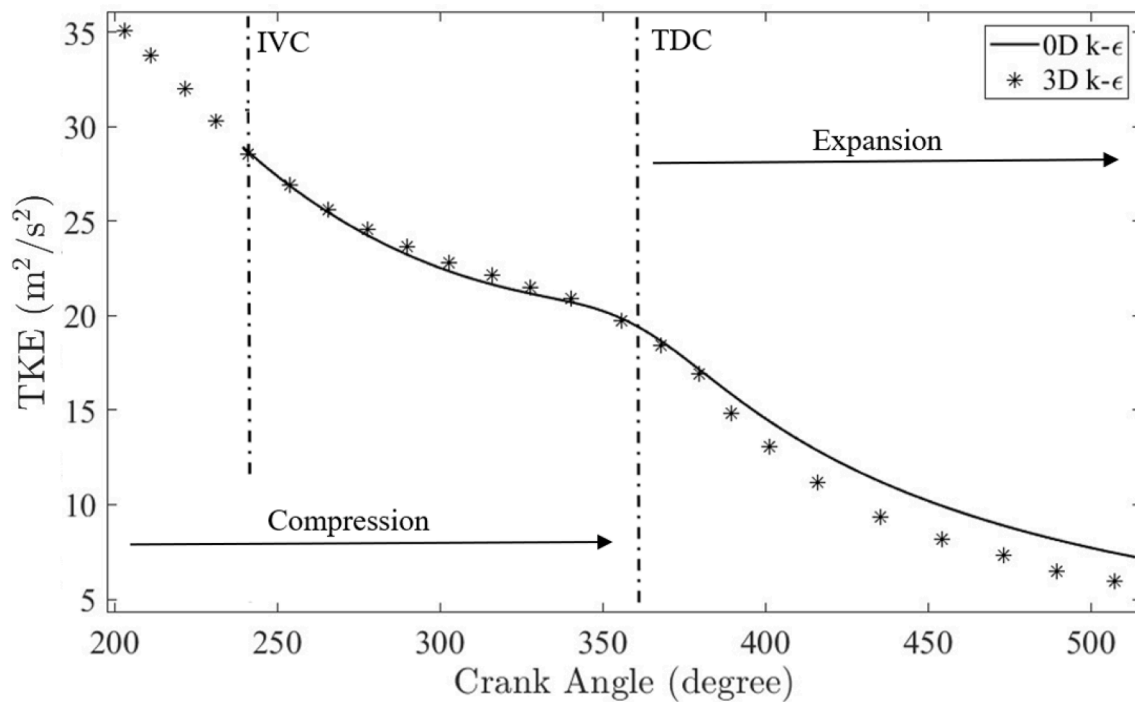


Fig. 2. Turbulent kinetic energy, TKE, with crank angle (MAP = 100 kPa, IVC = 240 ° CA, CR = 11.5).

et al. [33] showed that the knock in hydrogen ICE could be resulted from the spontaneous combustion of the end-gas mixture and the interaction of the pressure and flame waves. In this study, knock is based on the auto-ignition of an unburned end-gas reactive mixture at a particular pressure and temperature that was sufficient to initiate ignition after a delay time, τ . Knocking integral KI was modelled analytically by integrating the inverse of the hydrogen auto-ignition delay time, and knock was prone to occur when the integral (Eq. (10)) equals or exceeds unity,

$$KI = \frac{1}{6N} \int_{\theta_{IVC}}^{\theta} \frac{1}{\tau} d\theta, \quad (10)$$

where N is the engine speed, τ is the auto-ignition delay time, IVC is intake valve closing, and θ is the crank angle position. The hydrogen autoignition delay time τ at various pressures, temperatures, equivalence ratios, and water addition were evaluated numerically using the Converge software [31]. A constant volume homogeneous reactor model was used to solve the energy equations. The equivalence ratio, pressure, and temperature were assumed to be spatially uniform throughout the reactor. Hence, the purpose of the model was to estimate the progress of the kinetic reactions as a function of time. The autoignition delay time values were generated a reduced reaction kinetic mechanism [34]. The simulated data of the autoignition delay time at different unburned mixture temperatures, pressures, and water additions were fitted using a least squares algorithm to obtain an expression for each equivalence ratio considered. The unburned mixture temperature was calculated by using the two-zone hydrogen combustion model (see Appendix).

2.5. Engine simulation

For the engine simulation, the initial and boundary conditions for the boosted lean burn hydrogen model are experimentally derived [35]. Table 1 provides the values for spark timing, equivalence ratio, manifold air pressure and the percentage of water addition used in simulation. Also, the simulations were conducted at a constant compression ratio of 11.5 at an engine speed of 2000 rpm.

Table 1

Operating conditions used in the hydrogen engine numerical model.

Parameters	Values
Spark Timing (°CA bTDC)	20 to 0
Equivalence ratio (-)	0.5 to 0.9
MAP (kPa)	80 to 120
Water addition (% by volume)	0 to 8

Source: [35]

3. Results and discussion

3.1. Laminar flame speed at engine conditions

Laminar flame speed (LFS) is the most influential parameter for numerically modelling engines. Fig. 3 shows how the hydrogen LFS values are influenced by different temperatures and equivalence ratios at a pressure of 3 MPa (Fig. 3a), 5 MPa (Fig. 3b), and 7 MPa (Fig. 3c). It can be seen that the hydrogen LFS decreases significantly with decreasing equivalence ratio. At a pressure of 5 MPa and a temperature of 600 K, the hydrogen LFS decreased by 47 %, 58 %, and 84 % when the equivalence ratio was decreased from 0.9 to 0.7, 0.65, and 0.5, respectively. This was due to the reduction of the energy content when the mixture becomes leaner. Additionally, it can be seen from Fig. 3(a-c) that the hydrogen LFS decreases with increasing pressure under all the presented equivalence ratios. For an equivalence ratio of 0.9 at a temperature of 700 K, the hydrogen LFS decreased by 24 % and 40 % when the pressure was increased from 3 MPa to 5 MPa and 7 MPa, respectively. This reduction in the hydrogen flame speed with increasing pressure could be due to the pressure effect on the LFS explained by the reaction order n being less than two, given as $S_L = p^{0.5n-1}$; similar effects have been discussed in [36,37]. Conversely, it can be seen from Fig. 3(a-c) that the hydrogen LFS increased monotonically with increasing temperature under all presented equivalence ratios and pressures. For a pressure of 5 MPa and an equivalence ratio of 0.9, the hydrogen LFS increased by more than six times when the temperature was increased

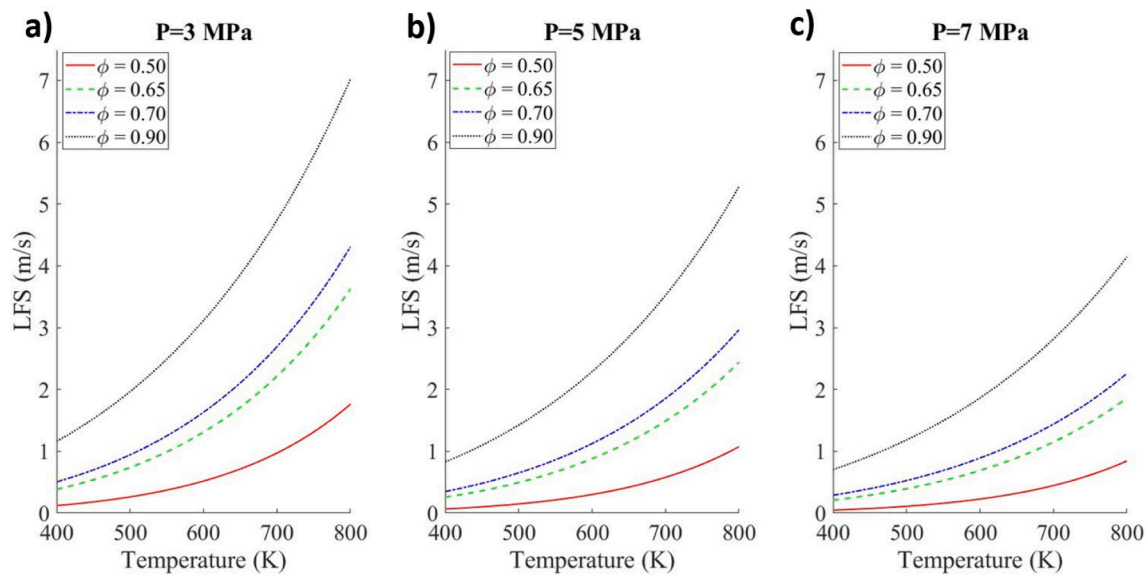


Fig. 3. Hydrogen laminar flame speed values at different temperatures, pressures and equivalence ratios. Calculated using hydrogen laminar flame speed empirical correlation [18].

from 400 K to 800 K. This was because the rate of the chemical reactions increases exponentially with increasing temperature based on the Arrhenius expression [24]. Fig. 4 presents how the LFS values at 4 MPa are influenced by water addition and temperature at an equivalence ratio of 0.5 (Fig. 4a), 0.65 (Fig. 4b), 0.7 (Fig. 4c), and 0.9 (Fig. 4d). It can be seen that the addition of water to a reactive hydrogen/air mixture causes the mixture LFS to reduce. For an equivalence ratio of 0.9 at a pressure of 40 bar and a temperature of 700 K, the LFS was reduced by 4

%, 13 %, 21 %, and 33 % when 1 %, 3 %, 5 %, and 8 % water was added, respectively. This was mainly due to the reduction of the global temperature and increased heat capacity of the hydrogen/air mixture with water addition [10]. It can be seen that the LFS correlation is sensitive for predicting the variations under different temperatures, pressures, equivalence ratios, and water additions, which is vital for numerical hydrogen engine combustion analysis.

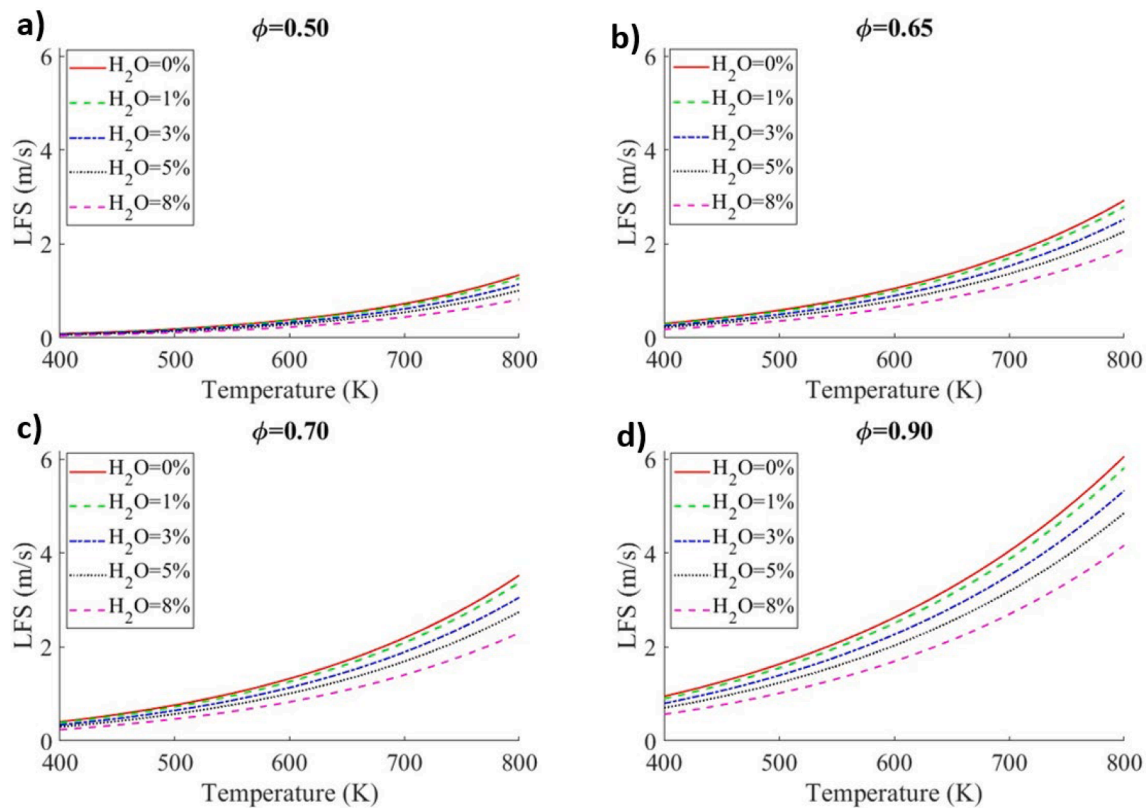


Fig. 4. Hydrogen laminar flame speed values at different equivalence ratios, temperature and water addition ($P = 4$ MPa). Calculated using hydrogen LFS empirical correlation [18].

3.2. Model validation

The developed two-zone hydrogen combustion model integrates LFS correlation [18], extended Zeldovich sub-models for NO prediction, and a reduced kinetics knock integral prediction in a boosted lean-burn hydrogen-fuelled SI engine with water addition. It was used to study the combustion performance under the operating conditions shown in Table 1. The simulated values of in-cylinder pressure at different equivalence ratios and spark timings were validated using experimental data [35]. The specifications of their engine and operating conditions are given in Table 2. In Fig. 5, the blue line and the blue marker represent the simulated results and experimental data for an equivalence ratio of 0.77, similarly the red line and the red marker correspond to an equivalence ratio of 0.5. The in-cylinder pressure shows that as the equivalence ratio decreases from 0.77 to 0.50, there is a significant reduction in the peak in-cylinder pressure as the crank angle corresponding of the peak in-cylinder pressure shifts away from top dead centre. This was mainly caused by the reduction of the hydrogen flame speed for greater air-diluted mixtures. At an equivalence ratio of 0.77, the peak pressure reaches approximately 4771 kPa, whereas at an equivalence ratio of 0.5, the peak pressure is around 3470 kPa. This reduction in peak pressure with decreasing equivalence ratio is consistent between the experimental and the simulated values. It can be seen that the developed model is capable of simulating the lean burn effects and the in-cylinder pressure values of lean burn hydrogen-fuelled SI engine with a high degree of accuracy.

3.3. Combustion characteristics

3.3.1. In-cylinder pressure

Fig. 6, shows that the simulated peak of in-cylinder pressure and apparent heat release rate (AHRR) decreases with an increase in water addition at a fixed engine speed of 2000 rpm and compression ratio of 11.5. Also, the crank angle associated with peak in-cylinder pressure shifts away marginally from TDC with water addition. For ϕ of 0.9, the crank angle corresponding to the maximum in-cylinder pressure shifts away from TDC by approximately 3 °CA for 8 % water addition compared to pure hydrogen operation; the magnitude of the peak also decreased from 5.52 MPa to 4.92 MPa. This decrease in magnitude of the in-cylinder peak pressure and the shift of the corresponding peak crank angle location are due to reduction in flame speed with water addition (Fig. 3 and Fig. 4). Similar outcomes were discussed in flames where the addition of water to hydrogen combustion controls the reaction rate and causes deflagration of lean burn hydrogen flames, eventually reducing the pressure rise [10].

The dilution effect also caused the peak AHRR to be decreased by 48 % when ϕ decreased from 0.9 to 0.5. Similarly, the peak AHRR also decreased with water addition. For ϕ of 0.9, the peak AHRR decreased by 5 % and 16 % when 3 % and 8 % of water addition, respectively. Additionally, the peak AHRR location shifted away from TDC by 2 °CA and 3 °CA when 3 % and 8 % water addition, respectively. The inset plot in Fig. 6 shows that the total AHRR decreased with decreasing equivalence ratio for both pure hydrogen combustion and hydrogen with water addition. This was due to reduction in flame speed for leaner hydrogen mixtures. The total AHRR decreased marginally with water addition. For ϕ of 0.9, the total AHRR decreased by 1 % and 7 % when 3 % and 8 % of

water addition, respectively. This reduction in the total heat release rate was due to reduced flame speed combined with an increase of the in-cylinder charge heat capacity with water addition. Fig. 7a shows the maximum in-cylinder pressure of a naturally aspirated hydrogen engine with differing amounts of water addition and varying equivalence ratios. The peak in-cylinder pressure magnitude of 5.2 MPa was found under an equivalence ratio of 0.9 for 40 kPa boosting. The maximum in-cylinder pressure reduces monotonically with increasing water addition for any given equivalence ratio. For an equivalence ratio of 0.9, the maximum in-cylinder pressure reduced by 1 %, 4 %, 6 %, and 10 % when 1 %, 3 %, 5 %, and 8 % water was added, respectively. However, the maximum in-cylinder pressure increased with increasing equivalence ratio under all simulated cases of water addition which was due to an increase in energy content from the higher concentration of hydrogen present in the mixture [38]. For pure hydrogen operation, the maximum in-cylinder pressure increased by 27 %, 45 %, and 55 % for equivalence ratios of 0.5 to 0.65, 0.77, and 0.9, respectively. Similarly, Fig. 7b shows the maximum in-cylinder combustion pressure increased as manifold absolute pressure (MAP) increased due to an increase in charge density [39]. For an equivalence ratio of 0.9, the maximum in-cylinder pressure increased by 8 % and 16 % as MAP increased from 80 kPa to 100 kPa and 120 kPa, respectively.

3.3.2. Indicated mean effective pressure

Optimal spark timing is mainly determined by the characteristics of the flame propagation within the combustion chamber and the associated engine parameters such as load, fuel composition, intake pressure, intake temperature, and engine speed. The spark timing was fixed at the minimum spark advance for best torque (MBT) location to ensure maximum thermal efficiency under all operating conditions. Therefore, the MBT timing at the highest indicated mean effective pressure (IMEP) was determined by varying the spark timing for naturally aspirated (MAP = 80 kPa) condition at various equivalence ratios (Fig. 8a). The MBT advances from TDC when the mixture becomes leaner. At $\phi = 0.9$, the MBT timing was at 4 °CA bTDC, whereas for ϕ of 0.5 it was at 10 °CA bTDC. This is explained by increased combustion duration due to the reduction of flame speed for leaner mixtures. Fig. 8a shows that IMEP reduced by 41 % when the ϕ reduced from 0.9 to 0.5 at their respective MBT timings under the naturally aspirated condition.

Fig. 8b shows the variation of IMEP at different MAP for different spark timings when $\phi = 0.77$. As MAP increased, the MBT timing shifted towards TDC due to the increased charge density at higher MAP values. When MAP increased from 80 kPa to 100 kPa and 120 kPa, the IMEP at MBT timing increased by 5 and 10 bar, respectively. The IMEP increase is explained by increased in-cylinder charge density for higher intake manifold air pressures [30]. Fig. 9 shows that for pure hydrogen under ϕ of 0.77 the MBT timing was found to be at 6 °CA bTDC, but for 3 % and 8 % water addition the MBT shifted marginally to 7 and 8 °CA bTDC, respectively. This was caused by an increase in combustion duration with water addition, due to a reduction in flame speed.

3.3.3. Burn-rate of hydrogen

The instantaneous mass fraction burned per crank angle for various equivalence ratios at a fixed spark timing of 5 °CA bTDC under naturally aspirated condition are shown in Fig. 10a. As air dilution in the hydrogen/air mixture increases, the combustion duration increases. The mass fraction burned is a good indicator of the engine performance. It is reasonable to use mass fraction burned curves to characterize the combustion stages as a function of crank angle. The crank angle location for 50 % (CA50) mass burn fraction shifted by 1, 2, and 6 °CA away with respect to the $\phi = 0.9$ condition, when the mixture tends to become leaner for equivalence ratio of 0.77, 0.65 and 0.5, respectively. In general, the CA50 location shifted away from TDC for leaner mixtures and caused by slower burning at increased air dilution, leading to an increase in combustion duration [6]. The effect of water addition on the hydrogen mass fraction burned (Fig. 10b), under naturally aspirated

Table 2
SI engine specifications used in simulations.

Characteristics	Values
Bore x stroke [m]	0.072 x 0.060
Displacement volume [m ³]	0.0002243
Compression ratio [-]	11.5
Speed [RPM]	2000

Source: [35]

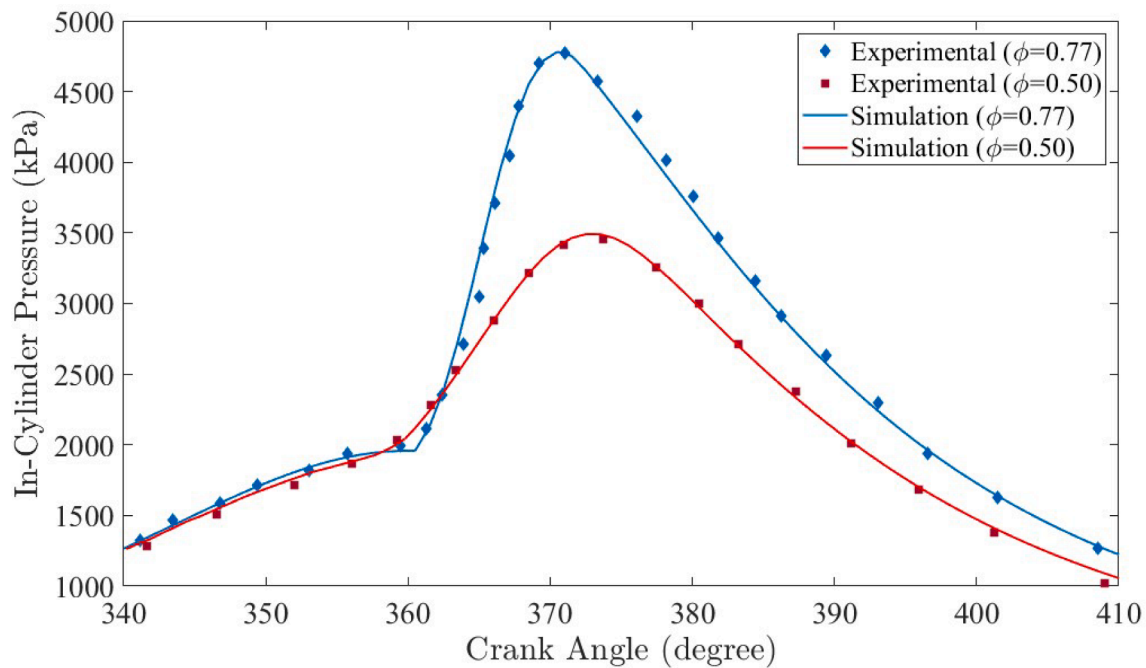


Fig. 5. The simulated in-cylinder pressure compared to experimental values of [35] (MAP = 84 kPa, CR = 11.5, N = 2000 rpm, $ST_{\phi=0.77}=3$ °CA bTDC, $ST_{\phi=0.50}=12$ °CA bTDC).

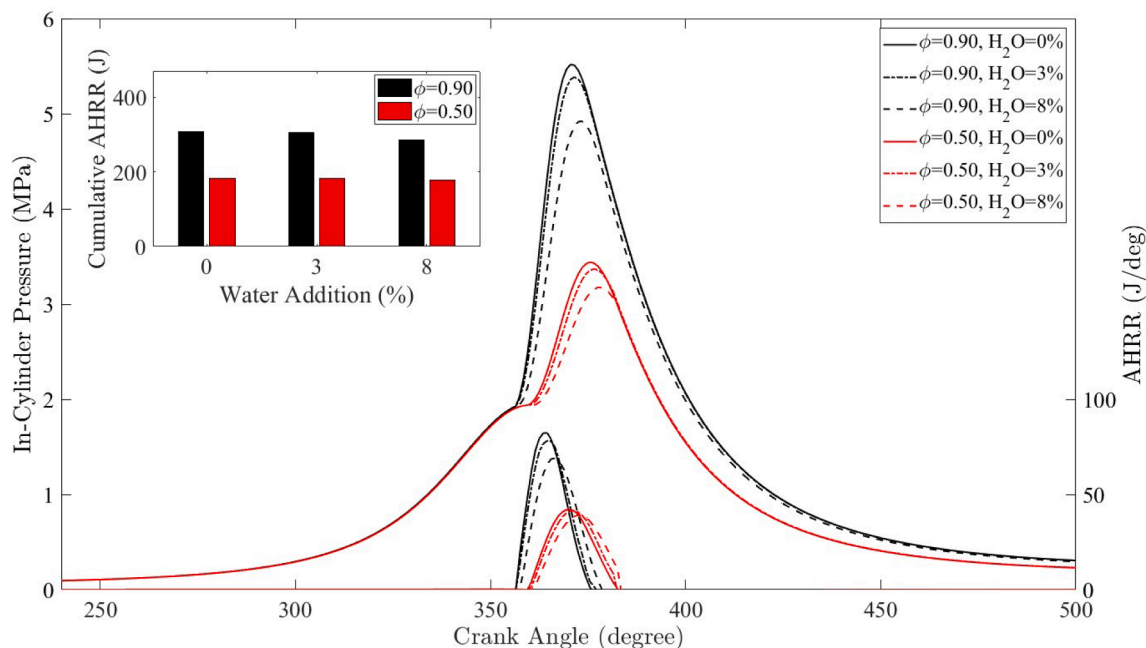


Fig. 6. Simulated hydrogen engine in-cylinder pressure and AHRR for various ϕ at different water additions (MAP = 80 kPa, CR = 11.5, ST = 350 ° CA bTDC).

condition at $\phi = 0.77$, was a marginally increased combustion duration. Water addition reduced the hydrogen flame speed, mostly due to the higher heat capacity hence a greater amount of heat was absorbed by the water inside the chamber. Therefore, the CA50 location shifted only by 3 °CA when 8 % water was added into the mixture. The water addition effect in the two-zone hydrogen combustion model was captured through the laminar flame speed effect and heat capacity variation caused by water addition.

After the evaluation of MBT timing for the conditions described in Table 1, the variation of IMEP for lean burn hydrogen engine at various MAP and ϕ at MBT timing were calculated (Fig. 11a), showing that

boosting increased the IMEP under all ϕ values. For ϕ of 0.9 the IMEP increased by 6 % and 13 % when MAP was increased from 80 kPa to 100 kPa and 120 kPa, respectively. For ϕ of 0.5, when the MAP increased from 80 kPa to 100 kPa, the IMEP increased by 4 bar. When MAP increased from 100 kPa to 120 kPa, the IMEP increased by 5 bar. Fig. 11b shows that water addition caused the IMEP of lean burn hydrogen engine load to decrease monotonically for all the presented equivalence ratios under naturally aspirated conditions. This is due to the reduction in the flame speed with water addition, which increases the combustion duration, leading to lower in-cylinder pressures. This new two-zone hydrogen combustion model was able to capture this

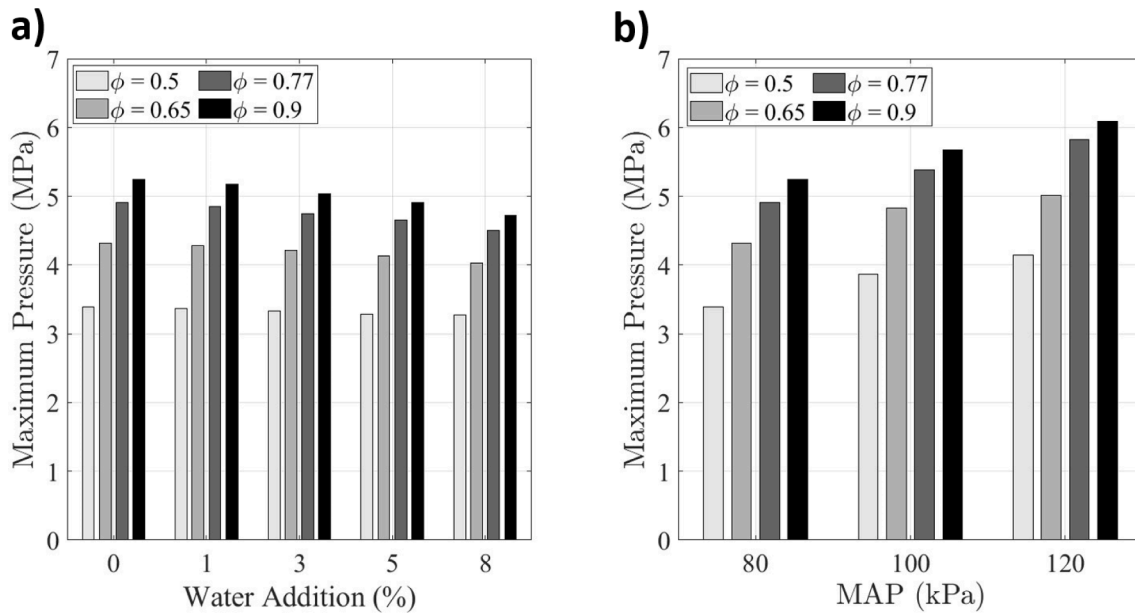


Fig. 7. a) The maximum in-cylinder pressure at various ϕ and water additions at naturally aspirated condition, MAP = 80 kPa, and b) the maximum in-cylinder pressure of pure hydrogen at various ϕ and MAP (ST = MBT, CR = 11.5).

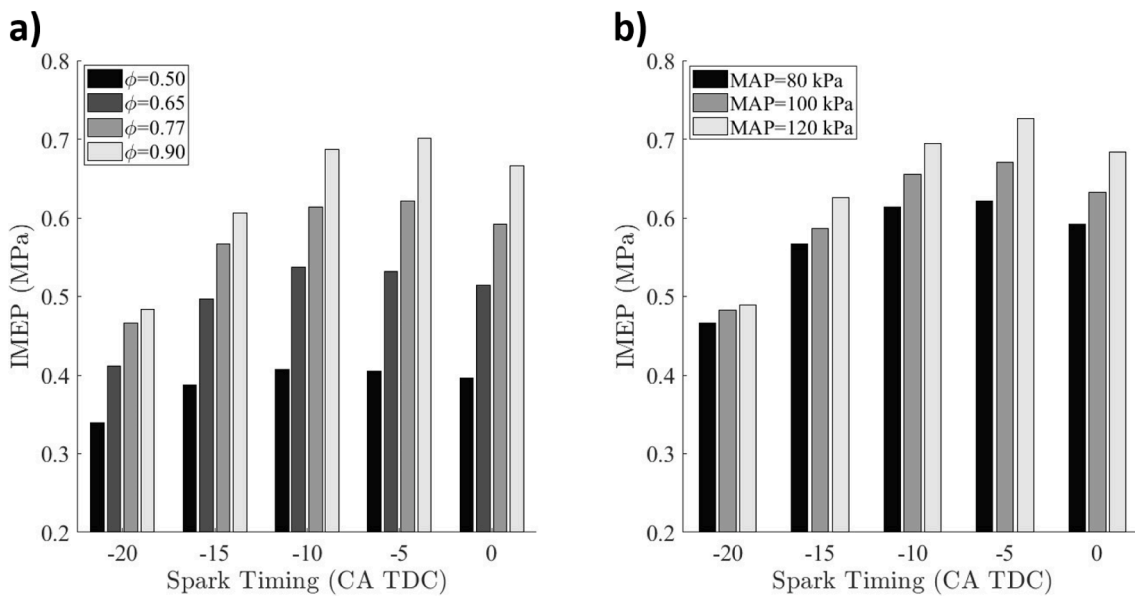


Fig. 8. a) Simulated IMEP at different spark timing for various equivalence ratios (MAP = 80 kPa) and, b) simulated IMEP at different spark timing for various manifold air pressures ($\phi = 0.77$).

effect only because of the incorporation a water-diluted hydrogen LFS correlation [18]. It can be seen from Fig. 11b that the rate of IMEP reduction with water addition was more important for greater equivalence ratio values. For ϕ of 0.9, the IMEP was reduced by 2 %, 6 %, 10 %, and 15 % when 1 %, 3 %, 5 %, and 8 % water was added, respectively. For leaner a ϕ value of 0.5 the IMEP was less affected by the water addition. The IMEP was reduced by 1 %, 3 %, 5 %, and 10 % when 1 %, 3 %, 5 %, and 8 % water was added, respectively. This decrease could be explained by the reduction of the global reaction temperature caused by the higher heat capacity of water vapor in the reactive mixture [40]. Additionally, the results also captured the lean burn hydrogen specific heat capacity variations caused by water addition through the incorporation of thermodynamic data of the NASA equilibrium program into the hydrogen combustion model [24]. In this work the water addition

was limited to 8 % because of the observed reduction in IMEP. Additional water dilution could impact the stability of hydrogen combustion, particularly in lean mixtures due to lower global temperatures, reduced reaction rates, and increased quenching distances, which collectively compromise combustion efficiency [41].

3.3.4. Indicated thermal efficiency

The quantification of the hydrogen thermal energy conversion into mechanical work is discussed using indicated thermal efficiency (ITE). The range of ITE for various MAP and ϕ is shown in Fig. 12a. It can be seen that the ITE increases with increasing air dilution. Under naturally aspirated condition, ITE increased by 4 %, 6 %, and 8 % when ϕ varied from 0.9 to 0.77, 0.65, and 0.5, respectively. The increase in ITE with decreasing fuel/air ratio was due to greater expansion of leaner mixtures

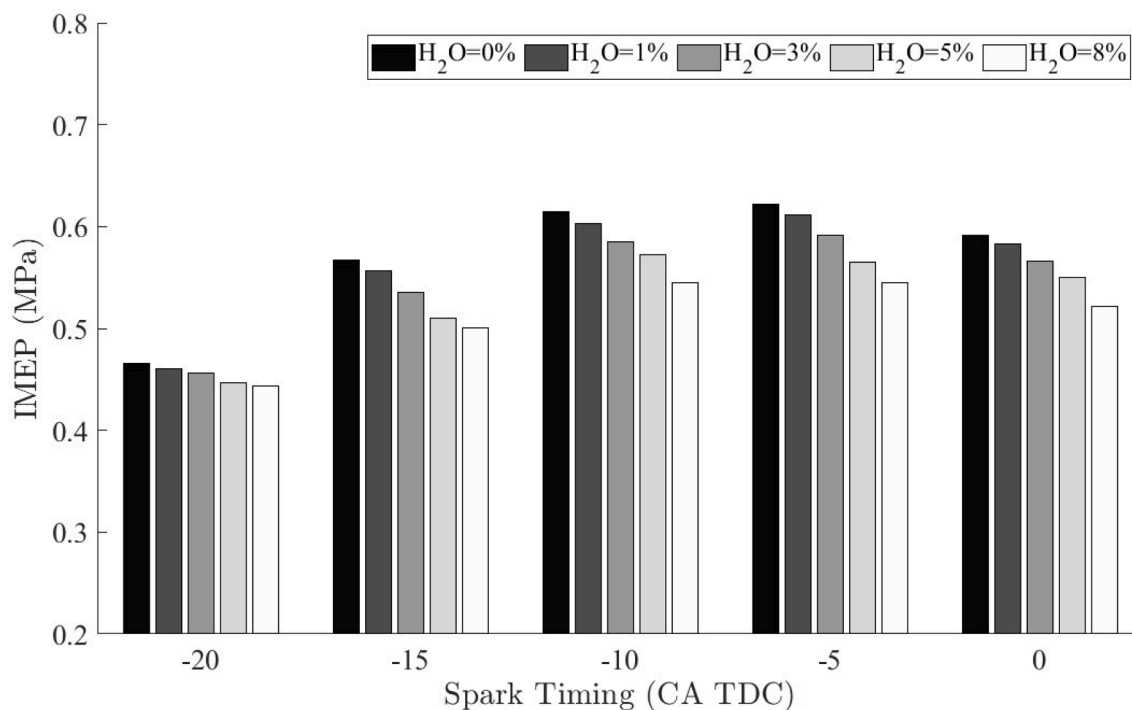


Fig. 9. Simulated IMEP at different spark timing for various percentages of water addition for $\phi = 0.77$ under naturally aspirated condition MAP of 80 kPa.

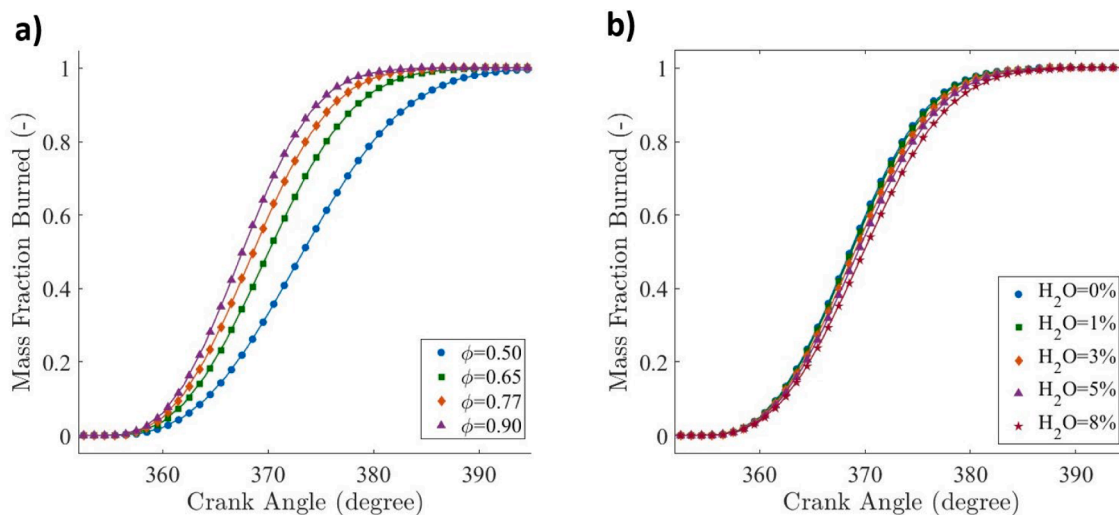


Fig. 10. a) Simulated mass fraction burned profile for various equivalence ratios at MAP = 80 kPa (CR = 11.5, N = 200 rpm, ST = 5° CA bTDC), and b) Simulated mass fraction burned profile for various water additions at MAP = 80 kPa (CR = 11.5, N = 200 rpm, ST = 5° CA bTDC).

caused by the variation of specific heat ratio [35]. Fig. 12a shows that for ϕ of 0.9, ITE increased by 3% and 7% when MAP increased (under naturally aspirated condition) to 100 kPa and 120 kPa, respectively. This increase can be attributed to an increase in IMEP with boosting (Fig. 11a). The peak ITE of nearly 42% were obtained under ϕ of 0.5 at 40 kPa boosting. Lean boosting has been shown to be an effective strategy to improve the ITE of hydrogen engines and commensurate with other studies [42–45]. In Fig. 12b, it can be seen that water addition caused a reduction in ITE for naturally aspirated lean burn hydrogen engine. This was attributed to the reduction in IMEP caused by the higher heat capacity of water, combined with the prolonged combustion duration due to reduction in hydrogen flame speed when water was added into the cylinder. For ϕ of 0.9, the ITE was reduced by 1%, 4%, 6%, and 10% when 1%, 3%, 5%, and 8% water was added, respectively.

The methodology does not account for the unburned hydrogen; however, the thermal efficiency reduces with equivalence ratio which increases engine-out unburned hydrogen [46].

3.4. Indicated specific fuel consumption and NO emissions

The indicated specific fuel consumption (ISFC) measures the effectiveness of the conversion thermal power of fuel to indicated power. Fig. 13a depicts the ISFC of a hydrogen-fuelled engine at various MAP and ϕ , at MTB timing, and shows that operating leaner reduces the ISFC due to the reduction in the amount of hydrogen in the in-cylinder mixture. Additionally, for ϕ of 0.9, the ISFC reduced by 3% and 8% when the MAP was increased from 80 to 100 and 120, respectively. The reduction in ISFC with boosting is due to increased indicated power at

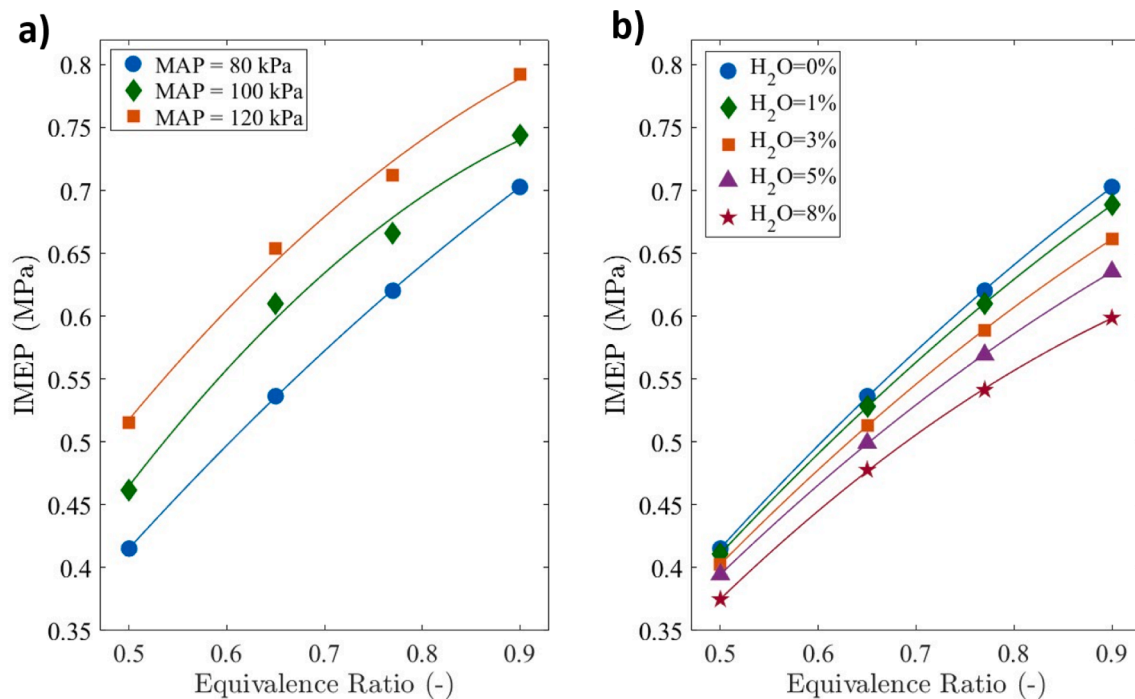


Fig. 11. a) IMEP at various MAP and ϕ . b) IMEP at various water additions and ϕ at naturally aspirated condition (CR = 11.5, MAP = 80 kPa, ST = MBT).

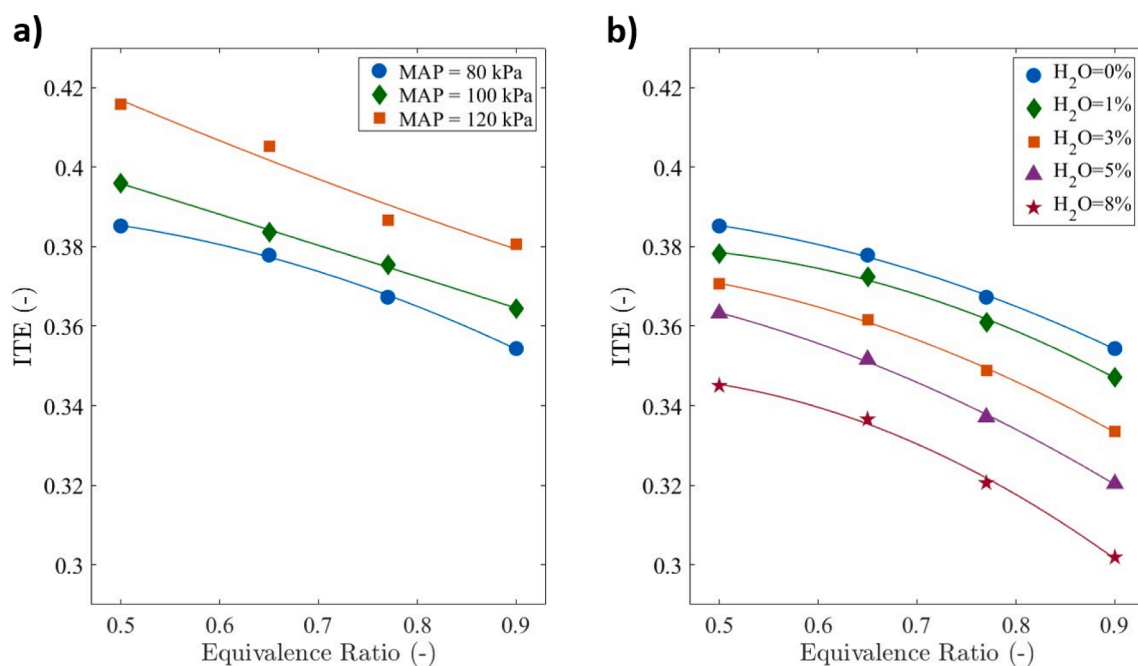


Fig. 12. a) ITE at various MAP and ϕ . b) ITE at various water additions and ϕ at naturally aspirated condition (CR = 11.5, MAP = 80 kPa, ST = MBT).

higher values of MAP, which also increases the in-cylinder charge density [47]. Similar results have been demonstrated experimentally in a boosted lean burn hydrogen SI engine [42].

In Fig. 13b, it can be seen that water addition under naturally aspirated conditions increases the ISFC monotonically under all presented equivalence ratios. This variation can be explained by the decrease in IMEP due to higher heat capacity and reduction of hydrogen flame speed caused by water addition [40]. Boosting decreased the ISFC, but NO emissions increased.

The amount of NO_x formed is dependent on the in-cylinder temperature, oxygen concentration, and reaction duration. Of the possible

NO_x emissions, nitric oxide (NO) is the important molecule released with the amount calculated by integrating the chemical rate equations of the extended Zeldovich mechanism [48]. Under ϕ of 0.9, NO emissions increased by 5% and 23% when the MAP was increased from 80 kPa to 100 kPa and 120 kPa, respectively. The increase in NO emissions with boosting is due to an increase in the in-cylinder charge density brought by greater energy content for higher MAP values at a given ϕ [49]. Hence, when the in-cylinder energy content was reduced by decreasing the equivalence ratio, for a given MAP significant reduction in NO emission was observed (Fig. 14a). For naturally aspirated conditions of 80 kPa, NO emissions were reduced by 39%, 55%, and 83% when ϕ

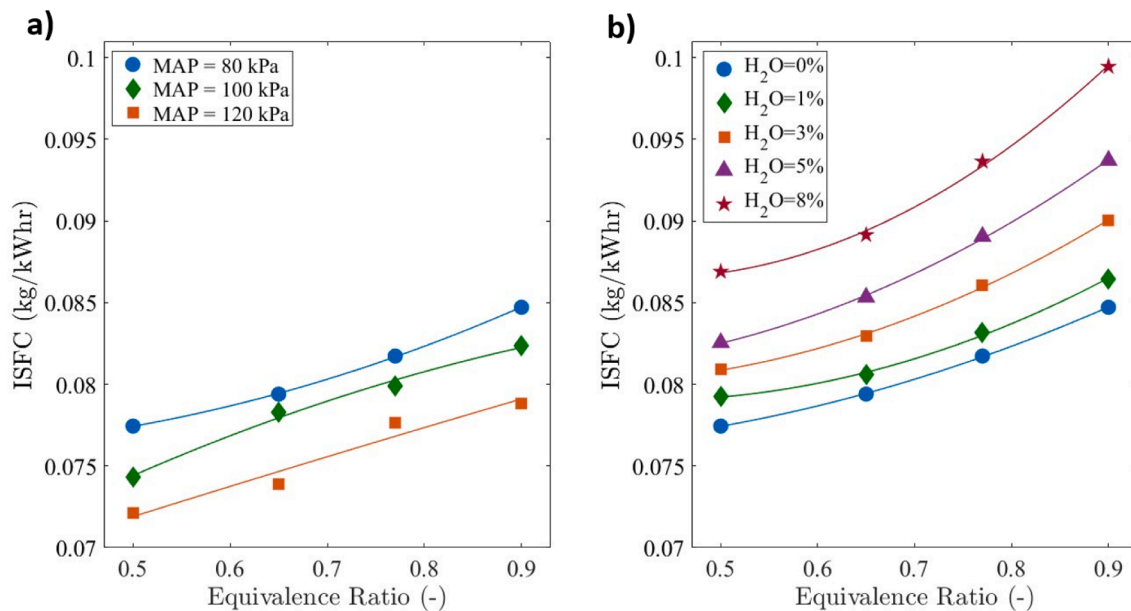


Fig. 13. a) ISFC at various MAP and ϕ . b) ISFC at various water additions and ϕ at naturally aspirated condition (CR = 11.5, MAP = 80 kPa, ST = MBT).

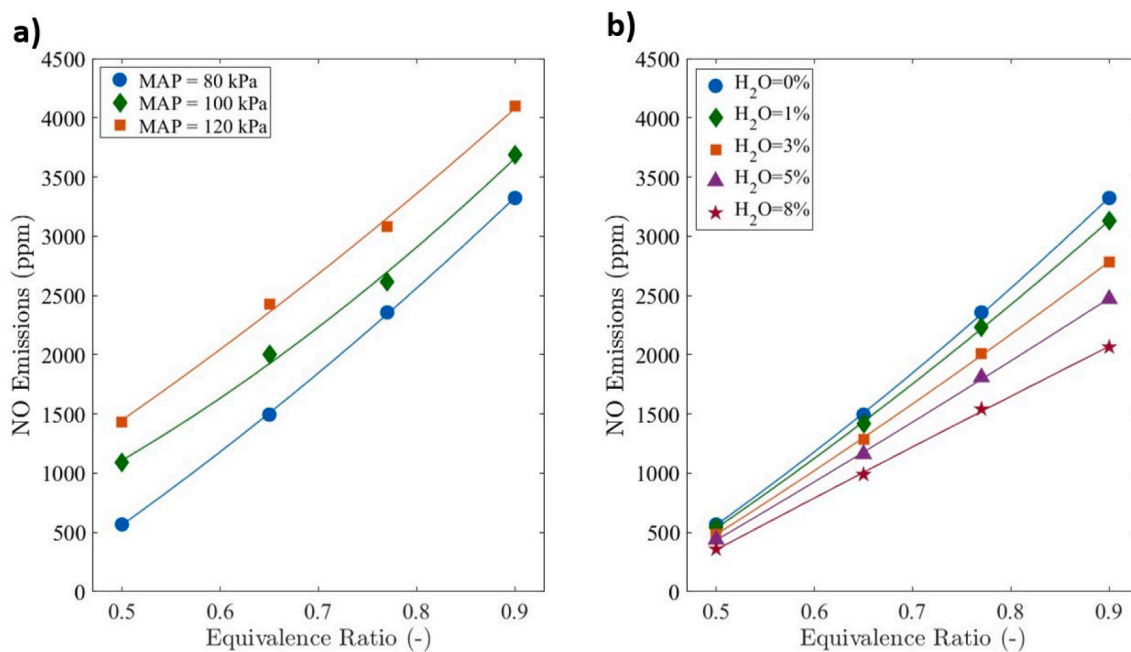


Fig. 14. a) NO emissions at various MAP and ϕ . b) NO emissions at various water additions and ϕ at naturally aspirated condition (CR = 11.5, MAP = 80 kPa, ST = MBT).

was varied from 0.9 to 0.77, 0.65, and 0.5, respectively. In contrast, for lean burn hydrogen engines, the addition of water increases ISFC but NO emissions reduced. This can be seen from Fig. 14b, where the NO emission decreased with decreasing values of ϕ and increasing values of water addition. For ϕ of 0.9, NO emissions were reduced by 6 %, 16 %, 26 %, and 38 % when 1 %, 3 %, 5 %, and 8 % water was added, respectively. This is mainly due to the reduction of the global in-cylinder temperature with water addition [14]. With current hydrogen SI engine technology, a compromise of load and NO emissions could be possible with the introduction of small percentages of water addition into the combustion chamber.

3.5. Knock prediction

The autoignition delay time is an important parameter for modelling combustion abnormalities. For the premixed fuel and oxidizer mixture, the ignition delay time is defined as the time from the start of spark to the initiation of chain-branching reactions [50]. The ignition delay time depends on equivalence ratio, pressure, temperature, and in-cylinder mixture concentration. Autoignition causes a rapid rise in cylinder pressure and this abnormal combustion is termed 'knock' [24]. In Fig. 15, the knock integral (KI) for lean burn hydrogen operation was calculated for various MAP and ϕ using the Livengood-Wu integral [51]. No end gas autoignition was observed for the operating conditions shown in Table 1, as none of the values exceeded unity and this was in

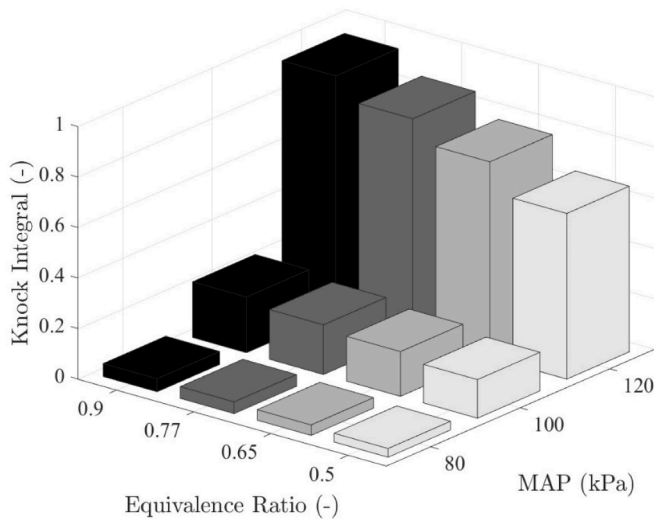


Fig. 15. Knock integral at various MAP and ϕ for hydrogen-fuelled SI engine at MBT timing ($N = 2000$ rpm, $CR = 11.5$).

line with experimental studies [5,49,52–54]. It is clear that when MAP was boosted, the KI increased significantly due to increase in the charge density as additional air is introduced into the combustion chamber. Additionally, knock could be mitigated by increased air dilution [53]. In Fig. 15, under MAP of 120 kPa, the KI was reduced by 8 %, 16 %, and 27 % when ϕ was varied from 0.9 to 0.77, 0.65, and 0.5, respectively. This reduction of the KI was caused by increased hydrogen autoignition delay time (Fig. 16). The autoignition delay time increased for higher levels of air-diluted hydrogen mixtures due to the reduction of the available energy in a reactive mixture.

The KI reduced monotonically with water addition (Fig. 17a) under all presented equivalence ratios under MAP of 120 kPa SI engine operation. For ϕ of 0.9, KI was reduced by 2 %, 6 %, 9 %, and 14 % when 1 %, 3 %, 5 %, and 8 % water was added, respectively. A slightly lower

reduction was observed for a leaner mixture; for ϕ of 0.5, the KI reduced by 2 %, 4 %, 6 %, and 10 % when 1 %, 3 %, 5 %, and 8 % water was added, respectively. This KI reduction with water addition was influenced by an increase in the hydrogen autoignition delay time with water addition (Fig. 17b). The hydrogen autoignition delay time increases with water addition due to the absorption of more heat by the higher heat capacity of water. Nevertheless, knocking and NO emissions in hydrogen-fuelled engines could be reduced but at the cost of engine performance. For a ϕ of 0.9 under a MAP of 120 kPa, if 1 % water was added, the KI and NO emissions reduced by 2 % and 5 %, respectively, while ITE was reduced by 2 %.

3.6. Hydrogen operational regimes

The outcomes from the developed two-zone hydrogen combustion model with water addition can be drawn together to describe the hydrogen engine performance, emissions, and combustion abnormalities. Fig. 18 illustrates the interaction between NO emissions, ISFC, IMEP, and the equivalence ratio of a hydrogen engine with different levels of water addition at a MAP of 120 kPa (Fig. 18a) and a MAP of 80 kPa (Fig. 18b). It can be seen from both maps that NO emissions and ISFC have an inversely proportional relationship when water is added to the hydrogen engine. This is because of the thermal efficiency reduction with water addition due to decrease in flame speed and an increase in the heat capacity of the in-cylinder charge. As the percentage of water increases, the NO emissions decrease significantly and is evident for all equivalence ratios. For ϕ of 0.9 at a MAP of 120 kPa (Fig. 18a), the NO emissions reduced by 35 % with 8 % water addition. This is due to the water addition lowering the in-cylinder combustion temperature, thereby reducing the formation of NO. However, reducing NO emission increases ISFC due to a reduction of the ITE (the dashed horizontal white lines in Fig. 18a and Fig. 18b). This reduction of thermal efficiency is due to lower combustion efficiency caused by higher values of specific heat capacity of the in-cylinder charge resulting from water addition and slower flame speeds. Note that the trade-off between ISFC and NO emissions is more dominant for richer mixtures, and it can be seen from the operational maps that the relation between ISFC and NO tends to

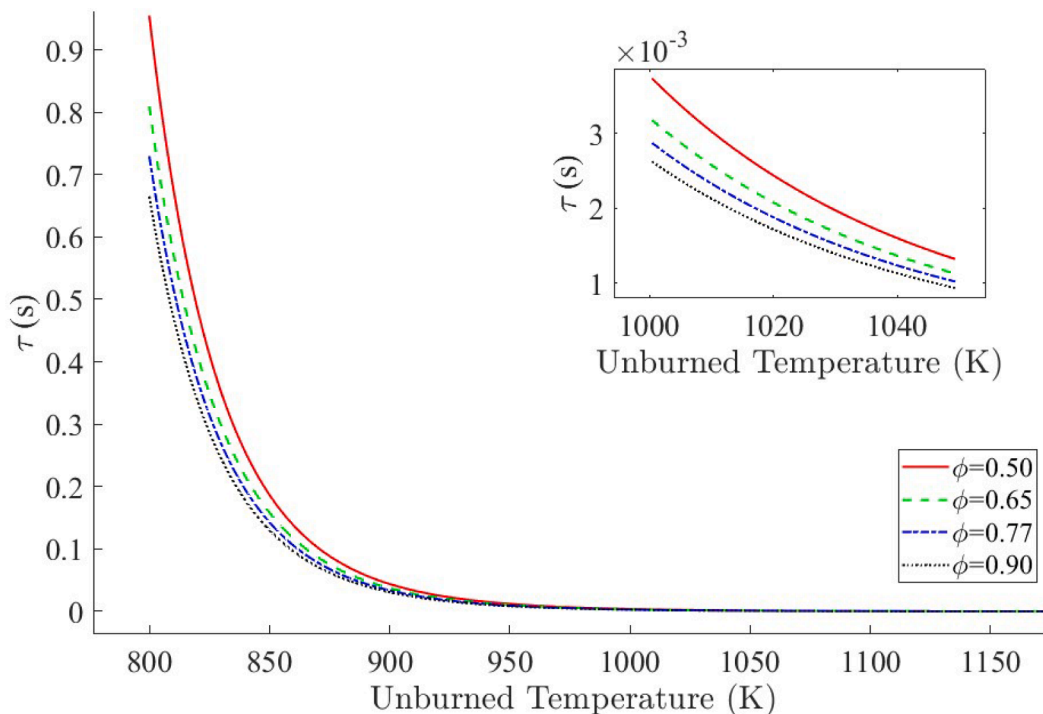


Fig. 16. Hydrogen autoignition delay time at various unburned gas temperature and ϕ ($P = 4$ MPa).

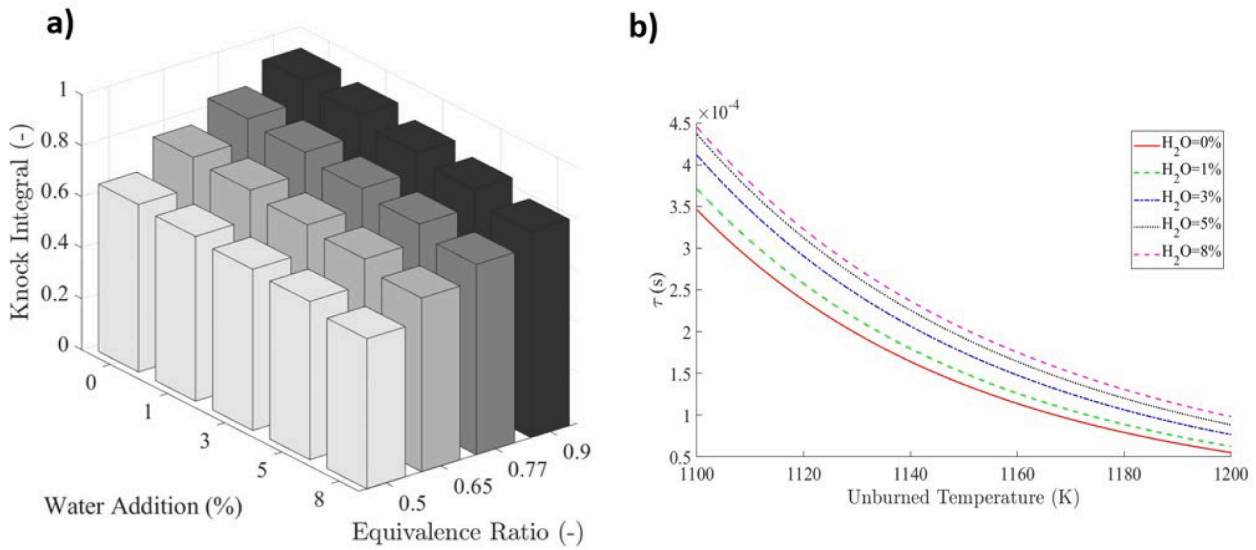


Fig. 17. a) Knock integral at various water additions and ϕ for hydrogen fuelled SI engine at MBT timing for naturally aspirated condition (CR = 11.5, MAP = 120 kPa). b) hydrogen autoignition delay time at various unburned gas temperature and water additions ($P = 4$ MPa, $\phi=0.9$).

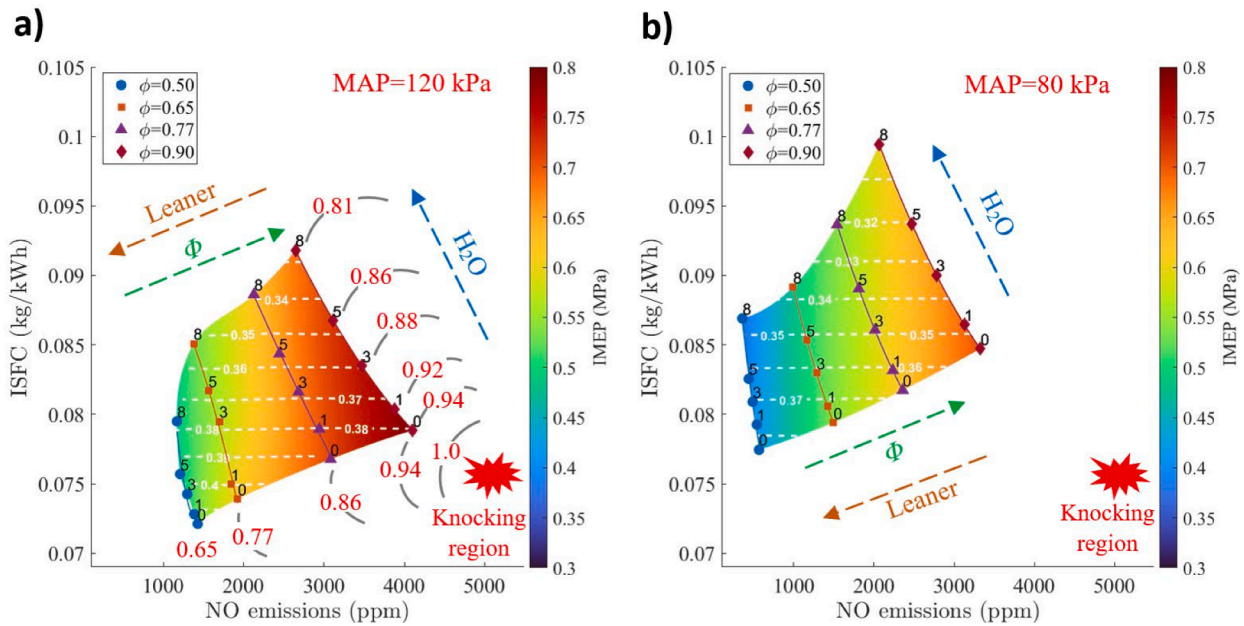


Fig. 18. Plots for the operation of a boosted lean burn hydrogen SI engine with water addition: a) at MAP of 120 kPa, and b) at MAP of 80 kPa. IMEP is shown as a heat map, in Fig. 18a and Fig. 18b). Higher IMEP values are associated with higher equivalence ratios, MAP, and lower percentages of water addition. However, the ITE increases with decreasing equivalence ratio. In Fig. 18a and Fig. 18b, the condition at which KI exceeds unity is highlighted as the 'knocking region'. The KI show that the knocking tendency increases with increasing equivalence ratio and load, whereas it decreases with water addition under all operating conditions. This is mainly due to the increase in hydrogen autoignition delay time with water addition. Hence, water injection could benefit hydrogen-fuelled engines by expanding the knock-free operating conditions at higher loads by reducing the knock tendency, but it comes with the trade-off of the reduced thermal efficiency thereby increasing the ISFC.

linearity as the hydrogen mixture became leaner. The colour map represents the IMEP (Fig. 18a and Fig. 18b). Higher IMEP values are associated with higher equivalence ratios, MAP, and lower percentages of water addition. However, the ITE increases with decreasing equivalence ratio. In Fig. 18a and Fig. 18b, the condition at which KI exceeds unity is highlighted as the 'knocking region'. The KI show that the knocking tendency increases with increasing equivalence ratio and load, whereas it decreases with water addition under all operating conditions. This is mainly due to the increase in hydrogen autoignition delay time with water addition. Hence, water injection could benefit hydrogen-fuelled engines by expanding the knock-free operating conditions at higher loads by reducing the knock tendency, but it comes with the trade-off of the reduced thermal efficiency thereby increasing the ISFC.

4. Conclusions

Incorporating the hydrogen LFS correlation, accounting for the water addition effect, in a two-zone combustion model serves a useful tool for investigating combustion, emission, and knocking characteristics of water-injected lean-burn boosted hydrogen SI engine. The addition of water to hydrogen engines offers the benefits of reducing combustion abnormalities and emissions. The water dilution effect is captured by thermal variations in the developed two-zone hydrogen combustion model. Water dilution increases the in-cylinder charge heat capacity and modulated the LFS within the combustion chamber, hence it reduces the NO emissions and mitigates the combustion abnormalities, but it also reduces ITE. The ITE reduces monotonically with water addition. For a ϕ of 0.9 under a MAP of 120 kPa, the addition of 1 % water caused the KI

and NO emissions to reduce by 2 % and 5 %, respectively, while ITE was reduced by 2 %. This study indicates that water addition could benefit hydrogen engine emission control and knock mitigation, but careful optimization is required to avoid significantly reducing thermal efficiency. The engine operation map based on ISFC, NO, ITE, ϕ and water addition obtained through this new two-zone model helps with the development of advanced combustion strategies in hydrogen internal combustion engines.

CRedit authorship contribution statement

D.N. Rrustemi: Writing – original draft, Visualization, Validation,

Appendix

A.1. Two-zone combustion model

After rearranging the equation of state, the first law and continuity equation, following first order differential equations were derived to model combustion process. The subscript u and b refer to unburned and burned zone respectively.

$$\frac{dT_u}{d\theta} = \frac{1}{m_u c_{pu}} \left(V_u \frac{dP}{d\theta} + \frac{dQ_u}{d\theta} \right)$$

$$\frac{dT_b}{d\theta} = \frac{1}{m_b c_{pb}} \left[P \frac{dV}{d\theta} - (R_b T_b - R_u T_u) \frac{dm_b}{d\theta} - \frac{R_u}{c_{pu}} \left(V_u \frac{dP}{d\theta} + \frac{dQ_u}{d\theta} \right) + V \frac{dP}{d\theta} \right]$$

$$\frac{dP}{d\theta} = \frac{1}{\frac{c_{vu}}{c_{pu}} V_u - \frac{c_{vb} R_u}{R_b c_{pu}} V_u + \frac{c_{vb}}{R_b} V} \left\{ \left(1 + \frac{c_{vb}}{R_b} \right) P \frac{dV}{d\theta} - \frac{dQ}{d\theta} + \left[(u_b - u_u) - c_{vb} \left(T_b - \frac{R_u T_u}{R_b} \right) \right] \frac{dm_b}{d\theta} + \left(\frac{c_{vu}}{c_{vb}} - \frac{c_{vb} R_u}{R_b c_{pu}} \right) \frac{dQ_u}{d\theta} \right\}$$

where T_u and T_b are the temperatures of the unburned and burned zones, respectively. θ is the crank angle, m_u and m_b are the masses of the unburned and burned gases, and c_{pu} is specific heat at constant pressure of the unburned mixture. The specific heat capacities c_{vu} and c_{vb} are at constant volume of the unburned and burned gases, respectively. The volume of the unburned zone is V_u and V is the volume of the combustion chamber. The in-cylinder pressure is P , and the gas constants of the unburned and burned gases are R_u and R_b , respectively. The terms $\frac{dQ_u}{d\theta}$ and $\frac{dQ}{d\theta}$ represent the rates of heat transfer in the unburned zone and total heat transfer, respectively. Finally, u_u and u_b are internal energy of the unburned and burned gases, respectively.

The following equations are used to account for convective heat transfer [24].

$$\frac{dQ}{d\theta} = \frac{dQ_u}{d\theta} + \frac{dQ_b}{d\theta}$$

$$\frac{dQ_u}{d\theta} = \frac{30A_u}{N} \left[h_{cu} (T_{gu} - T_w) + \beta \sigma (T_{gu}^4 - T_w^4) \right]$$

$$\frac{dQ_b}{d\theta} = \frac{30A_b}{N} \left[h_{cb} (T_{gb} - T_w) + \beta \sigma (T_{gb}^4 - T_w^4) \right]$$

where A is the surface area, h is convective heat transfer coefficient, β is a constant value of 0.6 and σ is Stefan-Boltzmann constant $5.67 \times 10^{-8} \text{ W/m}^2\text{K}^4$.

A.2. Laminar flame speed sub-model

The water diluted hydrogen laminar flame speed correlation according to [18];

$$S_l(\phi, P, T_u, \chi) = S_{l0}(\phi, P, T_u) \left(\frac{T_u}{T_0} \right)^{\alpha(\phi, P, T_u)} (1 - \chi^* F(\phi, P, T_u, \chi))$$

$$S_{l0} = a_1 \phi^2 + a_2 \phi^3 + a_3 \log_e(\phi) + a_4 \log_e \left(\frac{P}{P_0} \right) + a_5 \exp(-\phi) + a_6 \phi \log_e \left(\frac{P}{P_0} \right) + a_7 \log_e(\phi) \left(\frac{P}{P_0} \right) + a_8 \exp(-\phi) \left(\frac{P}{P_0} \right)$$

$$\alpha = \left(b_1 \phi^3 + b_2 \left(\frac{P}{P_0} \right)^3 + b_3 \phi^3 \left(\frac{P}{P_0} \right) + b_4 \log_e \left(\frac{P}{P_0} \right) + b_5 \exp(-\phi) + b_6 \phi \log_e \left(\frac{P}{P_0} \right) + b_7 \log_e(\phi) \left(\frac{P}{P_0} \right) + b_8 \exp(-\phi) \left(\frac{P}{P_0} \right) + b_9 \phi \exp \left(-\frac{P}{P_0} \right) \right) \exp \left(\beta \frac{T}{T_0} \right)$$

where P is pressure, T is temperature, P_0 is the reference pressure, T_0 is the reference temperature, χ is molar fraction, and β is dependent only on the equivalence ratio ϕ .

$$\beta = c_1 \phi^4 + c_2 \phi^3 + c_3 \phi^2 + c_4 \phi + c_5$$

Software, Methodology, Investigation, Formal analysis. **L.C. Ganippa:** Writing – review & editing, Supervision, Methodology, Conceptualization. **T. Megaritis:** Conceptualization. **C.J. Axon:** Writing – review & editing, Supervision, Project administration, Conceptualization.

Declaration of competing interest

The authors declare that they have no known competing financial interests or personal relationships that could have appeared to influence the work reported in this paper.

$$F = d_1 + d_2 \left(\frac{P}{P_0}\right) \chi^2 + d_3 \log_e \left(\frac{P}{P_0}\right) + d_4 \left(\frac{P}{P_0}\right)^2 \chi^2 + d_5 \left(\frac{T}{T_0}\right) + d_6 \left(\frac{P}{P_0}\right) \left(\frac{T}{T_0}\right) \chi^2 + d_7 \left(\frac{T}{T_0}\right) + d_8 \chi^2 \left(\frac{T}{T_0}\right) + d_9 \left(\frac{P}{P_0}\right)$$

Data availability

Data will be made available on request.

References

- [1] Bae C, Kim J. Alternative fuels for internal combustion engines. *Proc Combust Inst* 2017;36:3389–413. <https://doi.org/10.1016/j.proci.2016.09.009>.
- [2] Zaccardi J-M, Pilla G. Hydrogen as a Combustion Enhancer for Highly Efficient Ultra-Lean Spark-Ignition Engines. *SAE Tech Pap* 2019:2019-01-2258. <https://doi.org/10.4271/2019-01-2258>.
- [3] Mortimer J, Poursadegh F, Brear M, Yoannidis S, Lacey J, Yang Y. Extending the knock limits of hydrogen DI ICE using water injection. *Fuel* 2023;335:126652. <https://doi.org/10.1016/j.fuel.2022.126652>.
- [4] Berckmüller M, Rottengruber H, Eder A, Brehm N, Elsässer G, Müller-Alander G, et al. Potentials of a Charged SI-Hydrogen Engine. *SAE Tech Pap* 2003:2003-01-3210. <https://doi.org/10.4271/2003-01-3210>.
- [5] Xu H, Ni X, Su X, Xiao B, Luo Y, Zhang F, et al. Experimental and numerical investigation on effects of pre-ignition positions on knock intensity of hydrogen fuel. *Int J Hydrog Energy* 2021;46:26631–45. <https://doi.org/10.1016/j.ijhydene.2021.05.154>.
- [6] Rrustemi DN, Ganippa LC, Axon CJ. Investigation of boost pressure and spark timing on combustion and NO emissions under lean mixture operation in hydrogen engines. *Fuel* 2023;353:129192. <https://doi.org/10.1016/j.fuel.2023.129192>.
- [7] Dhyani V, Subramanian KA. Experimental investigation on effects of knocking on backfire and its control in a hydrogen fueled spark ignition engine. *Int J Hydrog Energy* 2018;43:7169–78. <https://doi.org/10.1016/j.ijhydene.2018.02.125>.
- [8] Krishnamoorthi M, Malayalamurthi R, He Z, Kandasamy S. A review on low temperature combustion engines: performance, combustion and emission characteristics. *Renew Sustain Energy Rev* 2019;116:109404. <https://doi.org/10.1016/j.rser.2019.109404>.
- [9] Zhang Q, Huang Z, Wang L, Lin G, Pan J. Experimental study of port water injection on GDI engine fuel economics and emissions. *ACS Omega* 2024;9: 8893–903. <https://doi.org/10.1021/acsomega.3c06859>.
- [10] Lyu Y, Qiu P, Liu L, Yang C, Sun S. Effects of steam dilution on laminar flame speeds of H₂/air/H₂O mixtures at atmospheric and elevated pressures. *Int J Hydrog Energy* 2018;43:7538–49. <https://doi.org/10.1016/j.ijhydene.2018.02.065>.
- [11] Subramanian V, Mallikarjuna J, Ramesh A. Effect of water injection and spark timing on the nitric oxide emission and combustion parameters of a hydrogen fuelled spark ignition engine. *Int J Hydrog Energy* 2007;32:1159–73. <https://doi.org/10.1016/j.ijhydene.2006.07.022>.
- [12] Younkings M, Wooldridge MS, Boyer BA. Port Injection of Water into a DI Hydrogen Engine. *SAE Tech Pap* 2015:2015-01-0861. <https://doi.org/10.4271/2015-01-0861>.
- [13] Younkings M, Wooldridge M, Boyer B. Direct In-cylinder Injection of Water into a PI Hydrogen Engine. *SAE Tech Pap* 2013:2013-01-0227. <https://doi.org/10.4271/2013-01-0227>.
- [14] Xu P, Ji C, Wang S, Cong X, Ma Z, Tang C, et al. Effects of direct water injection on engine performance in engine fuelled with hydrogen at varied excess air ratios and spark timing. *Fuel* 2020;269:117209. <https://doi.org/10.1016/j.fuel.2020.117209>.
- [15] Bleechmore C, Brewster S. Dilution Strategies for Load and NOx Management in a Hydrogen Fuelled Direct Injection Engine. *SAE Tech Pap* 2007:2007-01-4097. <https://doi.org/10.4271/2007-01-4097>.
- [16] Salek F, Babaie M, Hosseini SV, Bég OA. Multi-objective optimization of the engine performance and emissions for a hydrogen/gasoline dual-fuel engine equipped with the port water injection system. *Int J Hydrog Energy* 2021;46:10535–47. <https://doi.org/10.1016/j.ijhydene.2020.12.139>.
- [17] Kuppa K, Nguyen HD, Goldmann A, Korb B, Wachtmeister G, Dinkelacker F. Numerical modelling of unburned hydrocarbon emissions in gas engines with varied fuels. *Fuel* 2019;254:115532. <https://doi.org/10.1016/j.fuel.2019.05.115>.
- [18] Rrustemi DN, Ganippa LC, Megaritis T, Axon CJ. New laminar flame speed correlation for lean mixtures of hydrogen combustion with water addition under high pressure conditions. *Int J Hydrog Energy* 2024;63:609–17. <https://doi.org/10.1016/j.ijhydene.2024.03.177>.
- [19] Duva BC, Toulson E. Unstretched unburned flame speed and burned gas Markstein length of diluted hydrogen/air mixtures. *Int J Hydrog Energy* 2022;47:9030–44. <https://doi.org/10.1016/j.ijhydene.2021.12.217>.
- [20] Ma F, Li S, Zhao J, Qi Z, Deng J, Naeve N, et al. A fractal-based quasi-dimensional combustion model for SI engines fuelled by hydrogen enriched compressed natural gas. *Int J Hydrog Energy* 2012;37:9892–901. <https://doi.org/10.1016/j.ijhydene.2012.03.045>.
- [21] Demuyneck J, De Paep M, Huisseune H, Sierens R, Vancocillie J, Verhelst S. On the applicability of empirical heat transfer models for hydrogen combustion engines. *Int J Hydrog Energy* 2011;36:975–84. <https://doi.org/10.1016/j.ijhydene.2010.10.059>.
- [22] Woschni G. A universally applicable equation for the instantaneous heat transfer coefficient in the internal combustion engine. *SAE Tech Pap* 1967:670931. <https://doi.org/10.4271/670931>.
- [23] Krishnanunni J, Bhatia D, Das LM. Experimental and modelling investigations on the performance and emission characteristics of a single cylinder hydrogen engine. *Int J Hydrog Energy* 2017;42:29574–84. <https://doi.org/10.1016/j.ijhydene.2017.10.018>.
- [24] Heywood JB. *Internal combustion engine fundamentals*. New York: McGraw-Hill Education; 2018.
- [25] Yuan H, Giles K, Zhu S, Howson S, Lewis A, Akehurst S, et al. Kinetic modelling of combustion in a spark ignition engine with water injection. *Fuel* 2021;283:118814. <https://doi.org/10.1016/j.fuel.2020.118814>.
- [26] Ma F, Liu H, Wang Y, Wang J, Ding S, Zhao S. A Quasi-Dimensional Combustion Model for SI Engines Fuelled by Hydrogen Enriched Compressed Natural Gas. *SAE Tech Pap* 2008:2008-01-1633. <https://doi.org/10.4271/2008-01-1633>.
- [27] Conte E, Boulouchos K. A Quasi-Dimensional Model for Estimating the Influence of Hydrogen-Rich Gas Addition on Turbulent Flame Speed and Flame Front Propagation in IC-SI Engines. *SAE Tech Pap* 2005:2005-01-0232. <https://doi.org/10.4271/2005-01-0232>.
- [28] Blizard NC, Keck JC. Experimental and theoretical investigation of turbulent burning model for internal combustion engines. *AE Tech Pap* 1974:740191. <https://doi.org/10.4271/740191>.
- [29] Krebs S, Biet C. Predictive model of a premixed, lean hydrogen combustion for internal combustion engines. *Transp Eng* 2021;5:100086. <https://doi.org/10.1016/j.treng.2021.100086>.
- [30] Hunzinger N, Rothe M, Spicher U, Gegg T, Rieber M, Klimmek A, et al. Quasi-Dimensional Combustion Simulation of a Two-Stroke Engine. *SAE Tech Pap* 2006: 2006-32-0062. <https://doi.org/10.4271/2006-32-0062>.
- [31] Richards KJ, Senecal PK, Pomraning E. Converge 2023.
- [32] Salvi BL, Subramanian KA. A novel approach for experimental study and numerical modeling of combustion characteristics of a hydrogen fuelled spark ignition engine. *Sustain Energy Technol Assess* 2022;51:101972. <https://doi.org/10.1016/j.seta.2022.101972>.
- [33] Li Y, Gao W, Li Y, Fu Z, Zou J. Numerical investigation on combustion and knock formation mechanism of hydrogen direct injection engine. *Fuel* 2022;316:123302. <https://doi.org/10.1016/j.fuel.2022.123302>.
- [34] Villenave N, Dayma G, Brequigny P, Foucher F. Experimental measurements of ultra-lean hydrogen ignition delays using a rapid compression machine under internal combustion engine conditions. *Fuel* 2024;355:129431. <https://doi.org/10.1016/j.fuel.2023.129431>.
- [35] Sementa P, de Vargas Antolini JB, Tornatore C, Catapano F, Vaglieco BM, López Sánchez JJ. Exploring the potentials of lean-burn hydrogen SI engine compared to methane operation. *Int J Hydrog Energy* 2022;47:25044–56. <https://doi.org/10.1016/j.ijhydene.2022.05.250>.
- [36] Zhang W, Gou X, Kong W, Chen Z. Laminar flame speeds of lean high-hydrogen syngas at normal and elevated pressures. *Fuel* 2016;181:958–63. <https://doi.org/10.1016/j.fuel.2016.05.013>.
- [37] Kuznetsov M, Redlinger R, Breitung W, Grune J, Friedrich A, Ichikawa N. Laminar burning velocities of hydrogen-oxygen-steam mixtures at elevated temperatures and pressures. *Proc Combust Inst* 2011;33:895–903. <https://doi.org/10.1016/j.proci.2010.06.050>.
- [38] Oikawa M, Kojima Y, Sato R, Goma K, Takagi Y, Mihara Y. Effect of supercharging on improving thermal efficiency and modifying combustion characteristics in lean-burn direct-injection near-zero-emission hydrogen engines. *Int J Hydrog Energy* 2022;47:1319–27. <https://doi.org/10.1016/j.ijhydene.2021.10.061>.
- [39] Natkin RJ, Tang X, Boyer B, Oltmans B, Denlinger A, Heffel JW. Hydrogen IC Engine Boosting Performance and NOx Study. *SAE Tech Pap* 2003:2003-01-0631. <https://doi.org/10.4271/2003-01-0631>.
- [40] Law CK. *Combustion Physics*. 1st ed. Cambridge University Press; 2006. doi: 10.1017/CBO9780511754517.
- [41] Xu P, Ji C, Wang S, Cong X, Ma Z, Tang C, et al. Effects of direct water injection on engine performance in a hydrogen (H₂)-fuelled engine at varied amounts of injected water and water injection timing. *Int J Hydrog Energy* 2020;45:13523–34. <https://doi.org/10.1016/j.ijhydene.2020.03.011>.
- [42] Gürbüz H, Akçay İH. Evaluating the effects of boosting intake-air pressure on the performance and environmental-economic indicators in a hydrogen-fueled SI engine. *Int J Hydrog Energy* 2021;46:28801–10. <https://doi.org/10.1016/j.ijhydene.2021.06.099>.
- [43] Verhelst S, Maesschalck P, Rombaut N, Sierens R. Increasing the power output of hydrogen internal combustion engines by means of supercharging and exhaust gas recirculation. *Int J Hydrog Energy* 2009;34:4406–12. <https://doi.org/10.1016/j.ijhydene.2009.03.037>.
- [44] Luo Q, Hu J-B, Sun B, Liu F, Wang X, Li C, et al. Experimental investigation of combustion characteristics and NOx emission of a turbocharged hydrogen internal combustion engine. *Int J Hydrog Energy* 2019;44:5573–84. <https://doi.org/10.1016/j.ijhydene.2018.08.184>.

- [45] Lee J, Lee K, Lee J, Anh B. High power performance with zero NOx emission in a hydrogen-fueled spark ignition engine by valve timing and lean boosting. *Fuel* 2014;128:381–9. <https://doi.org/10.1016/j.fuel.2014.03.010>.
- [46] Chen Y, Jiang Y, Wen X, Liu H. An investigation of the kinetic modeling and ignition delay time of methanol–syngas fuel. *Front Energy Res* 2022;9:812522. <https://doi.org/10.3389/fenrg.2021.812522>.
- [47] Kneifel A, Buri S, Velji A, Spicher U, Pape J, Sens M. Investigations on supercharging stratified part load in a spray-guided DI SI engine. *SAE Int J Engines* 2008;1:171–6. <https://doi.org/10.4271/2008-01-0143>.
- [48] Knop V, Benkenida A, Jay S, Colin O. Modelling of combustion and nitrogen oxide formation in hydrogen-fuelled internal combustion engines within a 3D CFD code. *Int J Hydrog Energy* 2008;33:5083–97. <https://doi.org/10.1016/j.ijhydene.2008.06.027>.
- [49] Nguyen D, Choi Y, Park C, Kim Y, Lee J. Effect of supercharger system on power enhancement of hydrogen-fueled spark-ignition engine under low-load condition. *Int J Hydrog Energy* 2021;46:6928–36. <https://doi.org/10.1016/j.ijhydene.2020.11.144>.
- [50] Kuppa K, Goldmann A, Dinkelacker F. Predicting ignition delay times of C1-C3 alkanes/hydrogen blends at gas engine conditions. *Fuel* 2018;222:859–69. <https://doi.org/10.1016/j.fuel.2018.02.064>.
- [51] Livengood JC, Wu PC. Correlation of autoignition phenomena in internal combustion engines and rapid compression machines. *Symp Int Combust* 1955;5: 347–56. [https://doi.org/10.1016/S0082-0784\(55\)80047-1](https://doi.org/10.1016/S0082-0784(55)80047-1).
- [52] Lee K-J, Huynh TC, Lee J-T. A study on realization of high performance without backfire in a hydrogen-fueled engine with external mixture. *Int J Hydrog Energy* 2010;35:13078–87. <https://doi.org/10.1016/j.ijhydene.2010.04.078>.
- [53] Li Y, Gao W, Zhang P, Fu Z, Cao X. Influence of the equivalence ratio on the knock and performance of a hydrogen direct injection internal combustion engine under different compression ratios. *Int J Hydrog Energy* 2021;46:11982–93. <https://doi.org/10.1016/j.ijhydene.2021.01.031>.
- [54] Szwaja S, Bhandary K, Naber J. Comparisons of hydrogen and gasoline combustion knock in a spark ignition engine. *Int J Hydrog Energy* 2007;32:5076–87. <https://doi.org/10.1016/j.ijhydene.2007.07.063>.